Virology **277,** 420–428 (2000)
doi:10.1006/viro.2000.0625, available online at http://www.idealibrary.com on IDEAL®

Purified Recombinant Rotavirus VP7 Forms Soluble, Calcium-Dependent Trimers

Philip R. Dormitzer,*[,1] Harry B. Greenberg,†,‡ and Stephen C. Harrison*,§

*Laboratory of Molecular Medicine, Enders 673, Children's Hospital, 320 Longwood Avenue, Boston, Massachusetts 02115; †Department of Microbiology and Immunology and Department of Medicine, Stanford University School of Medicine, Stanford, California 94305; ‡the VA Palo Alto Health Care System, Palo Alto, California 94304; and §Howard Hughes Medical Institute and the Department of Molecular and Cellular Biology, Harvard University, 7 Divinity Avenue, Cambridge, Massachusetts 02138

Received July 5, 2000; returned to author for revision August 8, 2000; accepted August 22, 2000

Rotavirus is a major cause of severe, dehydrating childhood diarrhea. VP7, the rotavirus outer capsid glycoprotein, is a target of protective antibodies and is responsible for the calcium-dependent uncoating of the virus during cell entry. We have purified, characterized, and crystallized recombinant rhesus rotavirus VP7, expressed in insect cells. A critical aspect of the purification is the elution of VP7 from a neutralizing monoclonal antibody column by EDTA. Gel filtration chromatography and equilibrium analytical ultracentrifugation demonstrate that, in the presence of calcium, purified VP7 trimerizes. Trimeric VP7 crystallizes into hexagonal plates. Preliminary X-ray analysis suggests that the crystal packing reproduces the hexagonal component of the icosahedral lattice of VP7 on triple-layered rotavirus particles. These data indicate that the rotavirus outer capsid assembles from calcium-dependent VP7 trimers and that dissociation of these trimers is the biochemical basis for EDTA-induced rotavirus uncoating and loss of VP7 neutralizing epitopes.

Key Words: rotavirus; VP7; calcium; trimerization; assembly; purification; crystallization; uncoating; capsid; analytical ultracentrifugation.

INTRODUCTION

Rotavirus is the most important cause of severe, dehydrating childhood diarrhea worldwide (Committee, 1986). Two proteins, VP4 and VP7, are exposed on the surface of the triple-layered, icosahedral virion. VP4 forms spikes and is activated by trypsin cleavage to function as a fusion protein for cell entry (Estes *et al.,* 1981; Shaw *et al.,* 1993; Yeager *et al.,* 1994). VP7 is a calcium-binding glycoprotein that forms a thin outer layer with a $T = 13$ icosahedral lattice (Dormitzer and Greenberg, 1992; Prasad and Chiu, 1994; Yeager *et al.,* 1990). In a reconstructed image from electron cryomicroscopy, VP7 appears to form trimers on the surface of the virion (Yeager *et al.,* 1990). Both VP4 and VP7 are targets of neutralizing and protective antibodies against rotavirus (Hoshino *et al.,* 1985; Mackow *et al.,* 1988a,b; Offit *et al.,* 1986).

During viral replication, VP7 is retained in the lumen of the endoplasmic reticulum (ER), despite the removal of its only apparent transmembrane domain by signal cleavage (Clarke *et al.,* 1995; Maass and Atkinson, 1994). During viral assembly, the rotavirus double-layered particle buds from the low-calcium environment of the cytoplasm into the high-calcium environment of the ER lumen and acquires a transient envelope. The mature triple-layered virion is formed as the newly assembled outermost protein layer displaces the transient envelope. Double-layered particle budding and outer layer assembly are mediated by NSP4, a virally encoded nonstructural glycoprotein, which is anchored in the ER membrane, increases the permeability of the ER membrane to calcium, and forms a complex with double-layered particles, VP4, and VP7 (Maass and Atkinson, 1990; Au *et al.,* 1993; Tian *et al.,* 1995). When the ER is depleted of calcium, rotavirus maturation is blocked at the enveloped intermediate stage, and the outer layer does not form (Poruchynsky *et al.,* 1991).

During cell entry, the rotavirus triple-layered particle uncoats, losing VP4 and VP7, and the transcriptionally active double-layered particle is delivered into the cytoplasm. This membrane penetration event occurs in the context of passage from the high-calcium extracellular environment to the low-calcium environment of the cytoplasm. Raising the intracellular calcium concentration blocks entry (Ludert *et al.,* 1987).

The outermost layer of rotavirus contains calcium (Shahrabadi *et al.,* 1987). *In vitro,* calcium chelation triggers uncoating of the triple-layered particle (Cohen *et al.,* 1979). The sensitivity of virions to low concentrations of calcium has been linked genetically to VP7 (Gajardo *et al.,* 1997; Ruiz *et al.,* 1996). Expressed VP7, in the absence of other rotavirus proteins, undergoes an antigenic change upon calcium chelation, losing its ability to bind neutralizing monoclonal antibodies (mAbs) (Dormitzer and Greenberg, 1992).

[1] To whom correspondence should be addressed. Fax: (617) 738-0184. E-mail: dormitze@crystal.harvard.edu.

0042-6822/00 $35.00

These findings suggest that formation of the outer layer during viral assembly and loss of the outer layer during cell entry are mediated by a calcium-dependent conformational change in VP7. During viral replication, these changes take place in the context of membrane disruption.

Recombinant rhesus rotavirus (RRV) VP7 has been expressed in insect cells by a baculovirus vector (Fiore *et al.,* 1995). We have developed a rapid and gentle procedure for purifying this recombinant VP7 in quantities sufficient for detailed biochemical and structural study. We have analyzed purified VP7 by circular dichroism spectroscopy (CD), gel filtration chromatography, and equilibrium analytical ultracentrifugation to determine the biochemical basis for its calcium-dependent antigenic change.

RESULTS

Sequence of the RRV gene segment 9 clone

We determined the DNA sequence (GenBank Accession No. AF295303) of the cDNA clone of RRV gene segment 9 mRNA that was used by Fiori and co-workers (1995) to construct the recombinant baculovirus. The sequence, after PCR modification of the 5′ end as described (Fiore *et al.,* 1995), is predicted to encode full-length VP7, including the amino-terminal signal peptide. VP7 encoded by the modified gene has three amino acid differences from the protein encoded by a published sequence of pooled RRV gene segment 9 mRNA (Mackow *et al.,* 1988a). The changes are Cys to Phe at position 32, Ala to Thr at position 171, and Asn to Tyr at position 324. Each change replaces an amino acid encoded by the pooled mRNA with the corresponding residue in a consensus sequence of VP7s from G-type 3 rotaviruses (Nishikawa *et al.,* 1989).

Purification of VP7

VP7 was purified from recombinant baculovirus-infected Sf9 cell cultures as described under Materials and Methods. The key step in the purification was specific binding of VP7 to a mAb 159 column and its subsequent specific elution by EDTA (Fig. 1). When used in a single column purification, the mAb 159 column alone purified VP7 to greater than 95% (Fig. 1B, lanes 16–20) from a clarified cell culture medium in which VP7 made up a minor portion of the total protein (Fig. 1B, lane "PRE"). A con A affinity chromatography step was added prior to the mAb 159 column to prevent fouling of the antibody column with cell culture constituents. Unlike the antibody column, the con A column can be cleaned with relatively harsh reagents and is commercially available. A gel filtration step was added after the mAb 159 column to eliminate heterogeneity in the VP7 preparation that was apparent by gel filtration (see below) but not by Coomassie-stained SDS–PAGE.

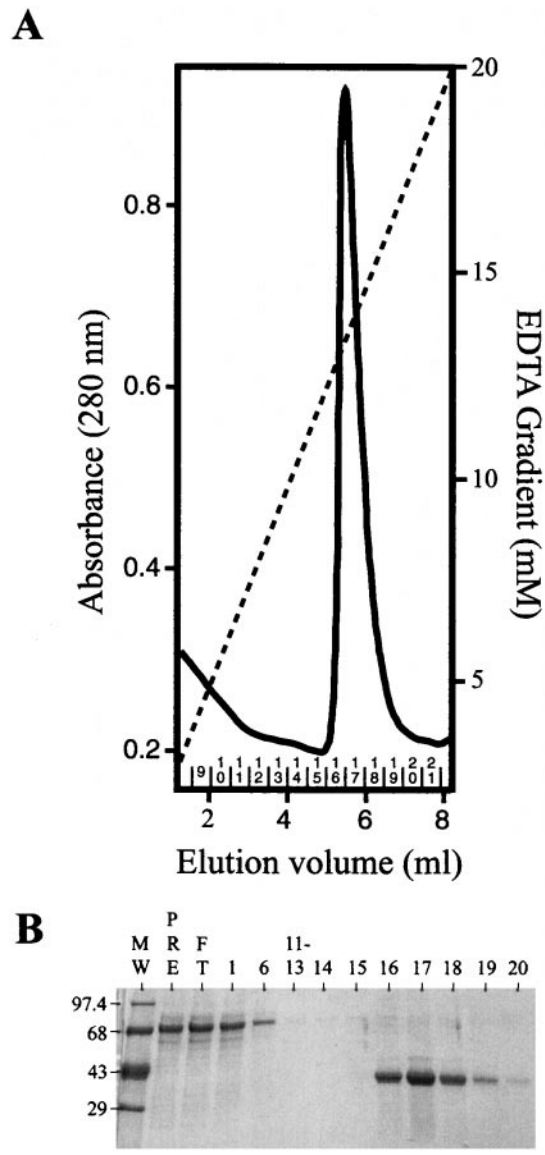

FIG. 1. Elution of VP7 from a mAb 159 column with an EDTA gradient. VP7 from clarified Sf9 cell culture medium was bound to the column and then eluted with a gradient from TNC to a buffer in which $CaCl_2$ was replaced by 20 mM EDTA. (A) Chromatogram during washing and elution. Solid line, A_{280} trace; dashed line, EDTA gradient; fraction numbers are above abscissa. The chromatogram was traced and scaled using Adobe Photoshop 5.0 and Adobe Illustrator 8.0. (B) Coomassie-stained 10–20% SDS–PAGE of eluted fractions. Lanes contain the following samples: MW, molecular weight standards (in kD); PRE, clarified cell culture medium; FT, flow-through; numbers refer to the eluate fractions indicated on the chromatogram. The major band in lanes PRE, FT, 1, and 6 derives from FBS in the baculovirus inoculum. The apparent MW of the VP7 band in lanes 16 to 20 is approximately 38 kD. The image was produced using Adobe Photoshop 5.0.

Two observations determined the choice of buffers used in the procedure. First, in the presence of EDTA, VP7 has a tendency to aggregate (see below). To minimize the amount of time that VP7 spent in the presence of excess EDTA, fractions from the mAb 159 column were collected in tubes containing 0.5 fraction vol. of buffer

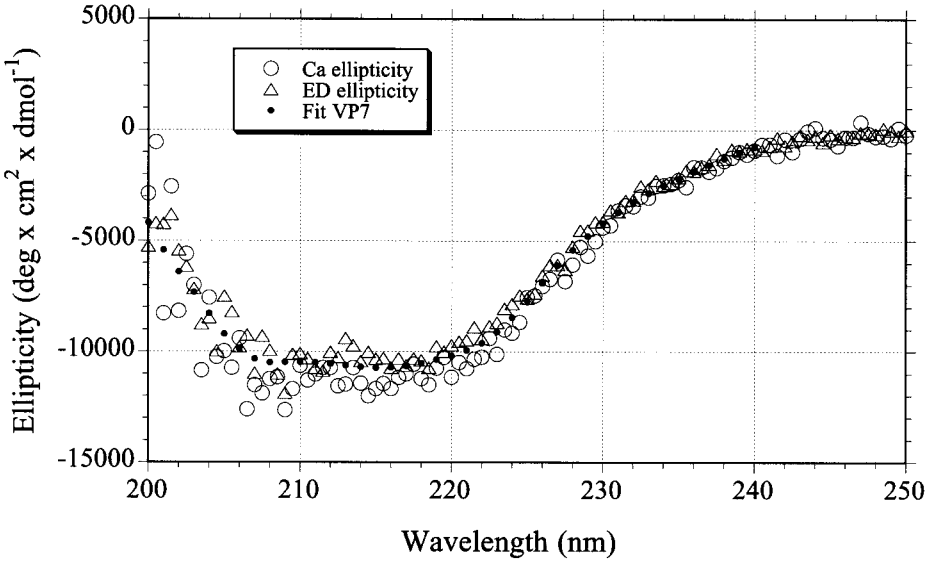

FIG. 2. CD spectroscopy of VP7. A reconstructed spectrum (Fit VP7) is superimposed on data sets collected at room temperature in the presence of either 1 mM $CaCl_2$ (Ca ellipticity) or 1 mM EDTA (ED ellipticity). Each data point is averaged from 12 measurements of 0.5 s each with a 1-nm bandwidth. Spectrum reconstructed using CONTIN (Provencher and Glockner, 1981).

with 5 mM calcium. Second, in the presence of calcium, VP7 tends to stick to surfaces; this tendency was less marked in 0.1 × TNC than in 1× TNC (data not shown). Therefore, prior to concentration by ultrafiltration, VP7 was dialyzed against 0.1 × TNC.

This procedure was effective at purifying VP7 from either Sf9 cell culture medium or lysed Sf9 cells. VP7 purified from a cell lysate produced a slightly more diffuse band by Coomassie-stained SDS–PAGE than did VP7 purified from the cell culture medium (not shown). No other significant differences were observed. The yield of purified VP7 was higher from the medium, with 0.25 to 0.5 mg obtained per liter of initial cell culture.

N-terminal sequencing of purified VP7

The identity of the purified protein was confirmed by amino acid sequencing. Efforts to determine the N-terminal sequence of the purified protein showed that the N-terminus was blocked. In rotavirus-infected cells, VP7 undergoes signal cleavage between residues Ala50 and Gln51, and the resulting N-terminus is blocked by pyroglutamic acid (Stirzaker *et al.,* 1987). Trypsin digestion of the purified protein produced a fragment with an apparent MW by SDS–PAGE of approximately 13.1 kDa and with an N-terminal sequence of "LVIT," corresponding to amino acids 224–227 of the predicted RRV VP7 amino acid sequence.

Mass spectroscopy of purified VP7

MALDI time-of-flight mass spectroscopy of purified recombinant VP7 yielded a main species with a MW of 32,154 (±64) and a minor species with a MW of 31,386 (±63). The predicted MW of RRV VP7 prior to signal cleavage is 36,992. After signal cleavage and modification of the N-terminus, but prior to glycosylation, the predicted MW of RRV VP7 is 31,229. RRV VP7 has one predicted N-linked glycosylation site at Asn69 (Mackow *et al.,* 1988a). The mass spectroscopy results are consistent with signal sequence cleavage, N-terminal modification, and glycosylation of the purified recombinant VP7.

Circular dichroism spectroscopy of VP7 in the presence of $CaCl_2$ and EDTA

To evaluate the possibility that calcium chelation induced a major rearrangement of secondary structure, CD spectra of VP7 were obtained from 200 to 240 nm in the presence of either 1 mM $CaCl_2$ or 1 mM EDTA. No significant differences were observed between the two spectra (Fig. 2). The data sets obtained with VP7 in $CaCl_2$- and EDTA-containing buffers were averaged, and the resulting data set was analyzed with the CONTIN software package (Provencher and Glockner, 1981). A spectrum representing 19% α-helix, 42% β-pleated sheet, 19% β-turn, and 20% disordered conformations gave an excellent fit to the experimental data (Fig. 2).

Gel filtration chromatography of VP7 in the presence of $CaCl_2$ and EDTA

The gel filtration profiles of VP7 in the presence of $CaCl_2$ and EDTA were very different (Fig. 3). Gel filtration of mAb 159-purified VP7 on a Superdex 200 column equilibrated in TNC produced two peaks. The major peak had a K_{AV} of 0.288, corresponding to an apparent MW of 141 kDa; the minor peak had a K_{AV} of 0.466, corresponding to an apparent MW of 46 kDa (Fig. 3A). The ratio of

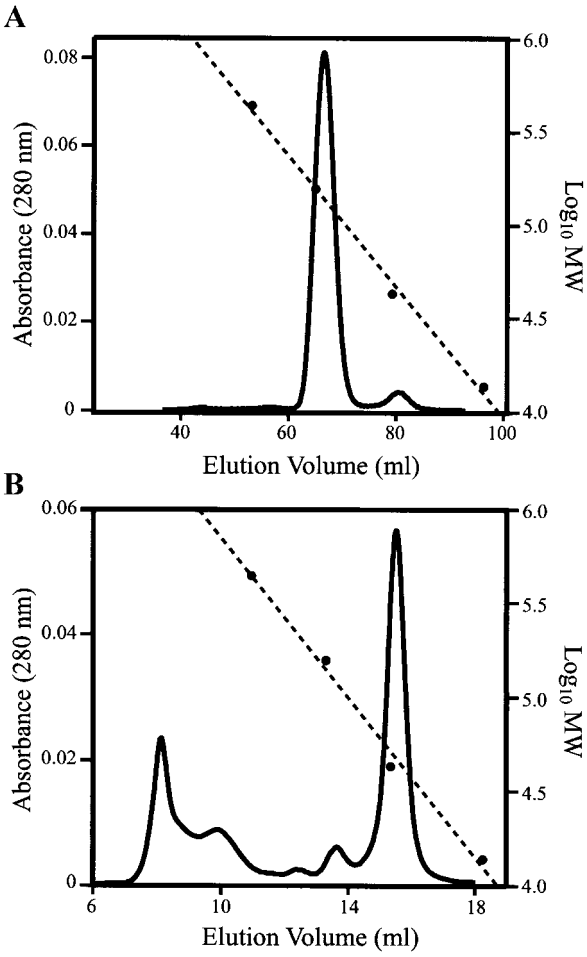

FIG. 3. Gel filtration chromatography of VP7. Solid lines, A_{280}; dashed lines, calibration curves; circles, elution volumes of MW markers. (A) Chromatogram from a Superdex 200 Hi-Load 16/60 gel filtration column equilibrated in TNC. Sample is the eluate from a mAb 159 column collected in tubes containing 0.5 fraction volumes of 5 mM $CaCl_2$. (B) Chromatogram from a Superdex 200 HR 10/30 gel filtration column equilibrated in TNE. Sample is the eluate of a mAb 159 column collected without adding excess calcium. Chromatograms were traced and scaled using Adobe Photoshop 5.0 and Adobe Illustrator 8.0.

apparent MWs of the major and minor peaks is 3.1 to 1. Protein harvested from the major calcium-associated VP7 peak did not change its gel filtration mobility after storage (not shown).

Gel filtration of mAb 159-purified VP7 on a Superdex 200 column equilibrated in TNE produced a major peak with a K_{AV} of 0.443, corresponding to an apparent MW of 47 kDa (Fig. 3B). At least four other peaks of VP7 eluted at lower volumes, including a peak in the void volume. Repeat gel filtration of protein harvested from the major EDTA-associated peak demonstrated an increasing proportion of higher MW complexes; repeat gel filtration of protein harvested from the high MW peaks demonstrated a relatively small amount of monomer (not shown). Gel filtration of VP7 in the presence of 5 mM $MgCl_2$ (not shown) yielded a pattern similar to that obtained in the presence of EDTA.

Analytical ultracentrifugation of VP7

VP7 from the major gel filtration peak in TNC was studied by equilibrium analytical ultracentrifugation (Fig. 4). When the equilibrium protein distributions from five starting concentrations were fit separately to models of single nonassociating proteins, the weight-average apparent MW increased from 79.4 kDa for the most dilute sample (51 μg/ml) to 96.2 kDa for the most concentrated sample (179 μg/ml). This increase suggested an associating system in dynamic equilibrium, with more oligomeric VP7 present at higher VP7 concentrations. Therefore, pooled data from the five samples were fit to models of a self-associating protein. The data predicted a 34.3 kDa protein that trimerizes with an association constant of approximately 2×10^3. In Fig. 4, an A_{280} vs radius curve predicted by this model is superimposed on one of the five data sets. The residuals between the data and the fit curve show a random scatter, demonstrating lack of evidence for either aggregation or nonideality in the sample.

Crystallization and preliminary X-ray analysis of VP7

VP7 was crystallized in the presence of calcium by the vapor diffusion method, as described under Materials and Methods. $CaCl_2$ concentration was a critical parameter. With less than 0.05 mM $CaCl_2$ in the crystallization buffer, crystals did not form reliably; with greater than 0.3 mM $CaCl_2$, many microcrystals formed. CsCl was included in the crystallization buffer because salts of alkali metals of high atomic mass promoted formation of isolated plates, while salts of alkali metals of lower atomic mass promoted formation of clustered plates and needles. Plates with partial or full hexagonal outline formed after 2 to 5 days of incubation at 30°C. These plates reached a maximum size of 640 by 250 μm but remained less than 25 μm thick. There were no significant differ-

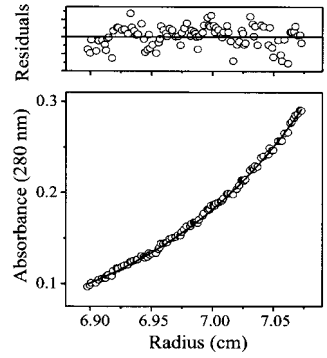

FIG. 4. Equilibrium analytical ultracentrifugation of VP7. A_{280} vs radius plot of 100 μg/ml VP7 in TNC following centrifugation at 9000 rpm at 4°C for 85 h. This protein distribution was stable over 30 h of measurements. The curve, fit to five data sets of VP7 at different concentrations, is the theoretical distribution of a 34.3-kDa protein with a K_{A3} of 1957 and a partial specific volume of 0.7223 ml/g in a buffer with a density of 1.004 g/ml. The baseline offset is 0.005 A_{280}.

ences in morphology between crystals of native and deglycosylated VP7.

X-ray diffraction with the incident beam perpendicular to the plane of the plates extended to spacings of 2.9 Å or smaller. The diffraction pattern revealed a well-ordered hexagonal lattice in the plane of the plates with $a = b = 114.0$ Å. X-ray beams parallel to the plane of the plates were diffracted with a highly elongated spot shape, except for a well-defined row of spots for reflections with $h = k = 0$. This row of spots indicated an interplanar spacing of 78.5 Å.

DISCUSSION

We have developed a rapid method for purifying recombinant VP7 expressed in Sf9 cells. The binding of neutralizing mAbs to recombinant rotavirus VP7 is calcium-dependent (Dormitzer and Greenberg, 1992). This observation suggested a straightforward and gentle purification strategy: bind expressed VP7 to a neutralizing mAb in the presence of calcium and elute it with EDTA. A similar approach has been used to purify clotting factors (Rudolph *et al.,* 1997; Takebe *et al.,* 1995). MAb 159 was selected for constructing the antibody affinity column because, in an ELISA format, it bound recombinant VP7 more stably than did other neutralizing mAbs tested (Dormitzer *et al.,* 1992). When used as a single chromatographic step, this antibody column yielded 0.25 to 0.5 mg of >95% pure VP7 per liter of starting insect cell culture (Fig. 1). This scale of production is sufficient to support both biochemical and X-ray crystallographic analysis.

In addition to simplicity and rapidity, this purification protocol has the advantage that specific calcium-dependent binding and release from mAb 159 selects for properly folded, mature VP7. When disulfide bond formation is blocked by DTT treatment of rotavirus-infected cells, neutralizing epitopes do not form (Svensson *et al.,* 1994). Similarly, a membrane-associated form of VP7 that is a precursor to mature VP7 in rotavirus-infected cells was not recognized by a neutralizing mAb (Kabcenell *et al.,* 1988). Therefore, forms of VP7 without mature disulfide bonds and the membrane-associated form of VP7 do not contaminate the preparations.

A reconstruction of the rotavirus triple-layered particle based on electron cryomicroscopy indicates that VP7 is arranged on the surface of the virion in trimers (Yeager *et al.,* 1990). Gel filtration chromatography demonstrates that purified calcium-bound VP7 also forms trimers in solution (Fig. 3A). In the presence of calcium, VP7 separates into major (141 kDa) and minor (46 kDa) peaks. The lack of VP7 eluting after the minor peak and the 3.1 to 1 ratio of apparent MWs of the major and minor peaks suggest that they contain soluble trimeric and monomeric VP7, respectively. The nonglobular shape of VP7, apparent in electron cryomicroscopy-based reconstructions of the virion (Prasad and Chiu, 1994; Yeager *et al.,* 1990), probably accounts for the difference between the apparent monomer MW of VP7 by gel filtration and its actual MW (32 kDa) determined by mass spectroscopy and calculated from its amino acid sequence.

Equilibrium analytical ultracentrifugation of calcium-bound VP7 from the major gel filtration peak confirmed the presence of trimers. The pooled data from samples with a range of VP7 concentrations fit a model of a 34-kDa protein in dynamic equilibrium between monomer and trimer. The estimate of monomer MW in this model is in good agreement with the true MW of the subunit. Attempts to fit the ultracentrifugation data to monomer–dimer or monomer–tetramer models of association did not yield correct predictions of monomer MW.

Circular dichroism spectroscopy and gel filtration chromatography clarify the biochemical basis for EDTA-induced virus uncoating and loss of VP7 neutralizing epitopes. There were no significant differences between the CD spectra of soluble VP7 in the presence of calcium or EDTA (Fig. 2). Therefore, a major calcium chelation-induced change in VP7 secondary structure is unlikely. In contrast, gel filtration chromatography demonstrated a major EDTA-induced change in the oligomeric state of VP7. In the presence of EDTA, there was a major peak with an apparent MW of 47 kDa (monomeric VP7) and a variety of higher molecular weight forms, which increased in proportion over time (Fig. 3B). These data indicate that calcium-free VP7 is predominantly monomeric, but aggregates over time.

X-ray crystallography has revealed two distinct structural roles for calcium in viral capsids. In polyoma viruses, such as SV40, calcium helps to bind together adjacent pentameric capsomeres by stabilizing tethering strands between them (Liddington *et al.,* 1991). In a number of plant viruses, such as tomato bushy stunt virus (TBSV), calcium binds together proteins within each trimeric capsomer by complexing negative charges at the interfaces of adjacent proteins (Hogle *et al.,* 1983). The biochemical data presented here indicate that calcium binds within VP7 trimers, probably assuming a structural role similar to that observed in the TBSV capsid.

The specificity of neutralizing mAbs for calcium-associated recombinant VP7 (Dormitzer and Greenberg, 1992) suggests that they specifically bind trimeric VP7. Neutralization escape mutant analysis shows that VP7's neutralizing epitopes are formed by amino acids that are widely spaced in VP7's primary sequence (Dyall-Smith *et al.,* 1986; Mackow *et al.,* 1988a; Taniguchi *et al.,* 1988). These residues may, in fact, be contributed by adjacent VP7 subunits at calcium-stabilized interfaces within trimers. Calcium chelation disrupts complexes of neutralizing mAbs and VP7 alone but not complexes of VP7-specific neutralizing mAbs and virions (Dormitzer *et al.,* 1994). Thus, neutralizing mAb binding of VP7 on the virion may

prevent the calcium chelation-induced dissociation of VP7 trimers.

Under standard biochemical conditions, neither gel filtration chromatography nor analytical ultracentrifugation reveals any evidence of higher order assemblies of calcium-bound, trimeric VP7. Similarly, electron microscopy of VP7 after EDTA treatment and negative staining with uranyl acetate (not shown) reveal no evidence for any ordered capsid-, sheet-, or tube-like structures, such as those observed with recombinant rotavirus VP6 (Estes *et al.,* 1987; Petitpas *et al.,* 1998). In contrast, under conditions of supersaturation, calcium-associated VP7 forms hexagonal plates. X-ray diffraction reveals a two-dimensional hexagonal unit cell length of 114 Å. Electron cryomicroscopy-based reconstructions of rotavirus particles show that the distance between 6-coordinated positions in the $T = 13$ icosahedral lattice is 110 to 120 Å at the radius of the VP7 layer (Prasad and Chiu, 1994; Yeager *et al.,* 1990). It is, therefore, likely that the lateral packing of VP7 is similar in the crystal and virion lattices.

The thickness of the VP7 layer on the virion is approximately 30 Å (Prasad and Chiu, 1994; Yeager *et al.,* 1990). The interplanar spacing of 78.5 Å in the crystals can, therefore, accommodate two layers, probably tail-to-tail (or head-to-head). These two-layer sheets must pack with perfect orientational register to yield the well-ordered hexagonal lattice observed by X-ray diffraction, but with considerable translational disorder parallel to the plane of the sheets. A hexagonal pattern of ridges and grooves can give rise to this sort of packing.

These experiments demonstrate that calcium-stabilized VP7 trimers are the basic building block of the outer layer of the rotavirus virion. VP7 can trimerize without binding to the trimeric VP6 pillars that make up the surface of the double-layered particle. Furthermore, these experiments indicate that dissociation of VP7 trimers is the biochemical basis for rotavirus uncoating and the loss of VP7 neutralizing epitopes triggered by calcium chelation. The tendency of VP7 to form well-ordered arrays should permit a high-resolution structure determination, either using X-ray diffraction by VP7 crystals with improved three-dimensional order or using electron diffraction by two-dimensional VP7 crystals.

MATERIALS AND METHODS

Cells, viruses, and antibodies

Sf9 insect cells were grown in Sf900II (Gibco BRL) and Excell 420 (JRH Biosciences) serum-free media. The recombinant baculovirus, which expresses RRV VP7 (G-type 3), was constructed by Fiore and coworkers (Fiore *et al.,* 1995). Baculovirus was propagated as previously described (Willis *et al.,* 1998). Baculovirus stocks were stabilized with 5–10% fetal bovine serum (FBS). Neutralizing mAb 159 has been previously described (Greenberg *et al.,* 1983) and was produced as a hybridoma culture supernatant. The hybridoma was grown in Hybridoma–SFM supplemented with OptiMAb enhancer (Gibco BRL).

Production of infected cell lysates and culture supernatants

Infection of Sf9 cells grown in spinner flasks with baculovirus was performed as previously described (Willis *et al.,* 1998). To recover VP7 from the medium of the infected cells, the medium was clarified by centrifugation at 2700 *g* for 10 min at 4°C and, in some preparations, by filtration through a 0.2-μM pore-size polyethylsulfone filter. Na-azide was added to 0.02%, and benzamidine was added to 2.5 mM. Alternatively, VP7 was released from the cell pellet by a single freeze-thaw in a lysis buffer consisting of phosphate-buffered saline (PBS), 1% Triton X-100, 5% glycerol, 0.02% Na-azide, 2.5 mM benzamidine, and 1 mM phenylmethylsulfonyl fluoride. The cell lysate was clarified by centrifugation at 235,000 *g* for 2 h at 4°C and diluted 10-fold with PBS, 0.02% Na-azide, and 0.5 mM benzamidine.

Preparation of the mAb 159 column

MAb 159 was partially purified by ammonium sulfate precipitation as previously described (Harlow and Lane, 1988). The antibody was then bound to Poros 20G beads (Perceptive Biosystems) in PBS, the beads were washed, and bound antibody was cross-linked to the beads using dimethylpimelimidate, as previously described (Parkhouse, 1984).

Purification of VP7

The clarified cell culture supernatant or cell lysate was passed over concanavalin A (Con A)–Sepharose beads (Amersham Pharmacia Biotech) at 4°C after equilibration of the column with 20 mM Tris, pH 8.0, 100 mM NaCl, 1 mM $CaCl_2$ (TNC). After the column was washed with TNC, VP7 was eluted at room temperature with TNC, 0.8 M methyl α-D-mannopyranoside.

The Con A column eluate was passed over a mAb 159 column that was mounted on a BioCad Sprint chromatography station (Perceptive Biosystems) and equilibrated with 20 mM Tris, pH 8.0, 50 mM NaCl, 0.1 mM $CaCl_2$ at room temperature. The column was washed with equilibration buffer, and VP7 was eluted with a step gradient to 20 mM Tris, pH 8.0, 50 mM NaCl, 1 mM EDTA. Eluted fractions were collected in tubes containing 0.5 fraction volumes of 20 mM Tris 8.0, 50 mM NaCl, 5 mM $CaCl_2$.

VP7 eluted from the mAb 159 column was buffer exchanged into 0.1× TNC by dialysis and concentrated by ultrafiltration (Amicon). Gel filtration chromatography was performed on an FPLC system at 4°C using Superdex 200 Hi-Load 16/60 or HR 10/30 gel filtration columns

(Amersham Pharmacia Biotech) equilibrated in 20 mM Tris, pH 8.0, 100 mM NaCl, 1 mM EDTA (TNE) or in TNC.

The above is an optimized VP7 purification protocol. Minor variations were used to produce some of the VP7 used in the experiments described in this report.

Quantitation of VP7

The concentration of VP7 was determined by spectrophotometry at 280 nm using a molar extinction coefficient of 61,270 M^{-1} cm^{-1}, calculated from the predicted amino acid sequence. For more accurate quantitation of the samples used in circular dichroism spectroscopy, the VP7 samples were diluted with 3 volumes of 8 M guanidine–HCl prior to spectrophotometry.

Amino acid sequencing

For N-terminal sequencing, 800 μg/ml of VP7 was digested with 2.5 μg/ml of L-(tosylamido 2-phenyl) ethyl chloromethyl ketone-treated trypsin (Worthington Biochemical) for 2 h at room temperature in TNE. The digestion was stopped with 1 mM PMSF. Digested fragments were separated by SDS–PAGE and electroblotted onto Sequi-Blot polyvinylidene difluoride membrane (Bio-Rad). Coomassie-stained bands were excised, and N-terminal sequence was obtained at the Tufts Protein Chemistry Facility (Boston).

Mass spectroscopy

A VP7 sample for mass spectroscopy was prepared by microdialysis against 1 mM $CaCl_2$. Matrix-assisted laser desorption (MALDI) time-of-flight mass spectroscopy was performed at the W. M. Keck Foundation Biotechnology Resource Laboratory at Yale University using a sinapinic acid matrix. The sample was calibrated using bovine serum albumin as a standard. The accuracy of measurement is estimated at $\pm$0.002%.

Circular dichroism spectroscopy

VP7 samples for CD were buffer exchanged by microdialysis into 20 mM boric acid–NaOH, pH 8.0, 100 mM NaF, with either 1 mM $CaCl_2$ or 1 mM EDTA. Circular dichroism was measured with an Aviv model 62DS CD spectrometer using a 1-mm path length quartz curvette.

Calibration of gel filtration columns

Superdex 200 gel filtration columns were calibrated using a set of globular protein standards (Amersham Pharmacia Biotech) consisting of ferritin (440 kDa), aldolase (158 kDa), ovalbumin (43 kDa), and RNase A (13.7 kDa). Calibration curves were constructed by plotting K_{AV} vs ln(MW), where $K_{AV} = (V_e - V_o)/(V_t - V_o)$. V_e is the measured elution volume of the markers; V_o, the void volume of the column, was determined by gel filtration of blue dextran; and V_t, the total column volume, was specified by the manufacturer (Amersham Pharmacia Biotech).

Analytical ultracentrifugation

Samples for analytical ultracentrifugation were microdialyzed against TNC. The diasylate was used as a blank and as a diluent for centrifugation. Analytical centrifugation was performed using an Optima XL-A analytical ultracentrifuge (Beckman Coulter). Absorbance data were obtained at 280 nm. Each sample was centrifuged at 9000 rpm in an AN-60 Ti rotor with six chamber centerpieces at 4°C for 85–91 h. The attainment of equilibrium was confirmed by comparing absorbance curves obtained at 6-h intervals. The specific volume of VP7 was calculated based on the amino acid composition of VP7, the carbohydrate content of VP7 (estimated by comparison of the predicted and mass spectroscopy-determined monomer MW of VP7), and published data (McRorie and Voelker, 1993). The density of TNC at 4°C was calculated from published data (McRorie and Voelker, 1993).

Crystallization of VP7

For crystallization, VP7 eluted from the mAb 159 column was dialyzed against 0.1× TNC, concentrated to 4 to 10 mg/ml using Centricon and Centriprep ultrafiltration units (Amicon), and gel filtered using Superdex 200 in 0.1× TNC. In some cases, the dialyzed, concentrated protein was incubated with glycopeptidase F (provided by Dr. Don Wiley) in a 1:460 to 1:1400 molar ratio for 2 h at 30°C prior to gel filtration. Crystals were obtained by the hanging-drop vapor diffusion method. VP7 at 6–8 mg/ml was mixed with an equal volume of 12–15% polyethylene glycol 10,000 MW (Hampton Research), 100–375 mM CsCl, 100 mM Pipes, pH 6.1, 0.1 mM $CaCl_2$, 0.02% sodium azide, 0.1 mM benzamidine in 2- to 8-μl drops. The crystallization trays were incubated at room temperature or at 30°C. Prior to freezing in liquid nitrogen, the crystals were soaked first in a solution in which CsCl was replaced with an equal concentration of NaCl and then in an equivalent solution containing 22–25% glycerol.

X-ray analysis

X-ray diffraction patterns of frozen crystals were obtained at the Cornell High Energy Synchrotron Source, beamline A1, with a Quantum-4 charge-coupled device detector (Area Detector Systems Corporation).

Molecular biology

Plasmid DNA for sequencing was prepared using Qiagen plasmid Midi kits. DNA oligonucleotide primer synthesis and plasmid DNA sequencing were performed by the Howard Hughes Medical Institute Biopolymer Facility

(Boston). SDS–PAGE, Coomassie staining, and electroblotting were performed using established techniques (Sambrook *et al.,* 1989). SDS–PAGE standards were obtained from Gibco BRL.

Computation

Image-plate X-ray diffraction data were processed using MOSFLM (Leslie, 1998). CD data were analyzed using CONTIN software, which uses a ridge regression algorithm to derive secondary structure predictions from CD spectra (Provencher and Glockner, 1981). A set of 16 proteins of known structure and polyglycolic acid were used as a comparison database (Sreerama and Woody, 1994). DNA and amino acid sequence data were analyzed using the Lasergene suite of sequence analysis software (DNAstar). Ultracentrifugation data were analyzed using Optima XL-A software version 3.0 (Beckman Instruments, Inc.) and Origin version 3.78 (Microcal Software). This software fits ultracentrifugation data to the model

$$A_r = A_{0,1}\exp[HM(x^2 - x_0^2)] + (A_{0,1})^N K \exp[HNM(x^2 - x_0^2)] + E,$$

where A_r is the absorbance at radius x; $A_{0,1}$ is the absorbance of the monomer at the reference radius x_0; H is a constant to account for the specific volume of the protein, the solvent density, the angular velocity of the rotor, and the temperature; M is the monomer molecular weight; N is the stoichiometry of the association; K is the association constant; and E is the baseline offset. $A_{0,1}$ is constrained to be greater than 0.

ACKNOWLEDGMENTS

We thank Marina Babyonyshev for technical assistance; John Rush of the HHMI Biopolymer Facility for DNA sequencing; Michael Berne of the Tufts Protein Chemistry Facility for N-terminal sequencing; Walter McMurray and Kathy Stone of the W. M. Keck Foundation Biotechnology Resource Laboratory for mass spectroscopy; and Raymond Brown, Susanne Liemann, Andrea Carfi, Stephen Litster, Mykol Larvie, Ernst Ter Har, Genfa Zhou, Ming Lei, and Yorgo Modis for helpful discussions.

This work was supported by National Institutes of Health Grant K08 AI 001496 to P.R.D., by Grant CA-13202 to S.C.H., and by a VA Merit Review Grant to H.B.G. S.C.H. is an investigator in the Howard Hughes Medical Institute.

REFERENCES

Au, K. S., Mattion, N. M., and Estes, M. K. (1993). A subviral particle binding domain on the rotavirus nonstructural glycoprotein NS28. *Virology* **194,** 665–673, doi:10.1006/viro.1993.1306.

Clarke, M. L., Lockett, L. J., and Both, G. W. (1995). Membrane binding and endoplasmic reticulum retention sequences of rotavirus VP7 are distinct: Role of carboxy-terminal and other residues in membrane binding. *J. Virol.* **69,** 6473–6478.

Cohen, J., Laporte, J., Charpilienne, A., and Scherrer, R. (1979). Activation of rotavirus RNA polymerase by calcium chelation. *Arch. Virol.* **60,** 177–186.

Committee on Issues and Priorities for New Vaccine Development. (1986). Appendix C: The burden of disease resulting from diarrhea. *In* "New Vaccine Development," Vol. II, "Diseases of Importance in Developing Countries," pp. 159–169. National Academy Press, Washington, DC.

Dormitzer, P. R., Both, G. W., and Greenberg, H. B. (1994). Presentation of neutralizing epitopes by engineered rotavirus VP7's expressed by recombinant vaccinia viruses. *Virology* **204,** 391–402, doi:10.1006/viro.1994.1543.

Dormitzer, P. R., and Greenberg, H. B. (1992). Calcium chelation induces a conformational change in recombinant herpes simplex virus-1-expressed rotavirus VP7. *Virology* **189,** 828–832.

Dormitzer, P. R., Ho, D. Y., Mackow, E. R., Mocarski, E. S., and Greenberg, H. B. (1992). Neutralizing epitopes on herpes simplex virus-1-expressed rotavirus VP7 are dependent on coexpression of other rotavirus proteins. *Virology* **187,** 18–32.

Dyall-Smith, M. L., Lazdins, I., Tregear, G. W., and Holmes, I. H. (1986). Location of the major antigenic sites involved in rotavirus serotype-specific neutralization. *Proc. Natl. Acad. Sci. USA* **83,** 3465–3468.

Estes, M. K., Crawford, S. E., Penaranda, M. E., Petrie, B. L., Burns, J. W., Chan, W. K., Ericson, B., Smith, G. E., and Summers, M. D. (1987). Synthesis and immunogenicity of the rotavirus major capsid antigen using a baculovirus expression system. *J. Virol.* **61,** 1488–1494.

Estes, M. K., Graham, D. Y., and Mason, B. B. (1981). Proteolytic enhancement of rotavirus infectivity: Molecular mechanisms. *J. Virol.* **39,** 879–888.

Fiore, L., Dunn, S. J., Ridolfi, B., Ruggeri, F. M., Mackow, E. R., and Greenberg, H. B. (1995). Antigenicity, immunogenicity and passive protection induced by immunization of mice with baculovirus-expressed VP7 protein from rhesus rotavirus. *J. Gen. Virol.* **76,** 1981–1988.

Gajardo, R., Vende, P., Poncet, D., and Cohen, J. (1997). Two proline residues are essential in the calcium-binding activity of rotavirus VP7 outer capsid protein. *J. Virol.* **71,** 2211–2216.

Greenberg, H. B., Valdesuso, J., van Wyke, K., Midthun, K., Walsh, M., McAuliffe, V., Wyatt, R. G., Kalica, A. R., Flores, J., and Hoshino, Y. (1983). Production and preliminary characterization of monoclonal antibodies directed at two surface proteins of rhesus rotavirus. *J. Virol.* **47,** 267–275.

Harlow, E., and Lane, D. (1988). "Antibodies: A Laboratory Manual." Cold Spring Harbor Laboratory Press, Cold Spring Harbor, NY.

Hogle, J., Kirchhausen, T., and Harrison, S. C. (1983). Divalent cation sites in tomato bushy stunt virus: Difference maps at 2.9 A resolution. *J. Mol. Biol.* **171,** 95–100.

Hoshino, Y., Sereno, M. M., Midthun, K., Flores, J., Kapikian, A. Z., and Chanock, R. M. (1985). Independent segregation of two antigenic specificities (VP3 and VP7) involved in neutralization of rotavirus infectivity. *Proc. Natl. Acad. Sci. USA* **82,** 8701–8704.

Kabcenell, A. K., Poruchynsky, M. S., Bellamy, A. R., Greenberg, H. B., and Atkinson, P. H. (1988). Two forms of VP7 are involved in assembly of SA11 rotavirus in endoplasmic reticulum. *J. Virol.* **62,** 2929–2941.

Leslie, A. G. W. (1988). MOSFLM, Version 5.51. Cambridge, UK.

Liddington, R. C., Yan, Y., Moulai, J., Sahli, R., Benjamin, T. L., and Harrison, S. C. (1991). Structure of simian virus 40 at 3.8-A resolution. *Nature* **354,** 278–284.

Ludert, J. E., Michelangeli, F., Gil, F., Liprandi, F., and Esparza, J. (1987). Penetration and uncoating of rotaviruses in cultured cells. *Intervirology* **27,** 95–101.

Maass, D. R., and Atkinson, P. H. (1990). Rotavirus proteins VP7, NS28, and VP4 form oligomeric structures. *J. Virol.* **64,** 2632–2641.

Maass, D. R., and Atkinson, P. H. (1994). Retention by the endoplasmic reticulum of rotavirus VP7 is controlled by three adjacent amino-terminal residues. *J. Virol.* **68,** 366–378.

Mackow, E. R., Shaw, R. D., Matsui, S. M., Vo, P. T., Benfield, D. A., and Greenberg, H. B. (1988a). Characterization of homotypic and heterotypic VP7 neutralization sites of rhesus rotavirus [published erratum appears in **Virology** (1988) **167,** 660]. *Virology* **165,** 511–517.

Mackow, E. R., Shaw, R. D., Matsui, S. M., Vo, P. T., Dang, M. N., and Greenberg, H. B. (1988b). The rhesus rotavirus gene encoding protein VP3: Location of amino acids involved in homologous and heterologous rotavirus neutralization and identification of a putative fusion region. *Proc. Natl. Acad. Sci. USA* **85,** 645–649.

McRorie, D. K., and Voelker, P. J. (1993). "Self-Associating Systems in the Analytical Ultracentrifuge." Beckman Instruments, Fullerton, CA.

Nishikawa, K., Hoshino, Y., Taniguchi, K., Green, K. Y., Greenberg, H. B., Kapikian, A. Z., Chanock, R. M., and Gorziglia, M. (1989). Rotavirus VP7 neutralization epitopes of serotype 3 strains. *Virology* **171,** 503–515.

Offit, P. A., Shaw, R. D., and Greenberg, H. B. (1986). Passive protection against rotavirus-induced diarrhea by monoclonal antibodies to surface proteins vp3 and vp7. *J. Virol.* **58,** 700–703.

Parkhouse, R. M. (1984). Immunopurification. *Br. Med. Bull.* **40,** 297–301.

Petitpas, I., Lepault, J., Vachette, P., Charpilienne, A., Mathieu, M., Kohli, E., Pothier, P., Cohen, J., and Rey, F. A. (1998). Crystallization and preliminary X-ray analysis of rotavirus protein VP6. *J. Virol.* **72,** 7615–7619.

Poruchynsky, M. S., Maass, D. R., and Atkinson, P. H. (1991). Calcium depletion blocks the maturation of rotavirus by altering the oligomerization of virus-encoded proteins in the ER. *J. Cell Biol.* **114,** 651–656.

Prasad, B. V., and Chiu, W. (1994). Structure of rotavirus. *Curr. Top. Microbiol. Immunol.* **185,** 9–29.

Provencher, S. W., and Glockner, J. (1981). Estimation of globular protein secondary structure from circular dichroism. *Biochemistry* **20,** 33–37.

Rudolph, A. E., Mullane, M. P., Porche-Sorbet, R., and Miletich, J. P. (1997). Expression, purification, and characterization of recombinant human factor X. *Protein Express. Purif.* **10,** 373–378.

Ruiz, M. C., Charpilienne, A., Liprandi, F., Gajardo, R., Michelangeli, F., and Cohen, J. (1996). The concentration of Ca^{2+} that solubilizes outer capsid proteins from rotavirus particles is dependent on the strain. *J. Virol.* **70,** 4877–4883.

Sambrook, J., Fritsch, E. F., and Maniatis, T. (1989). "Molecular cloning: A Laboratory Manual," 2nd ed. Cold Spring Harbor Laboratory Press, Cold Spring Harbor, NY.

Shahrabadi, M. S., Babiuk, L. A., and Lee, P. W. (1987). Further analysis of the role of calcium in rotavirus morphogenesis. *Virology* **158,** 103–111.

Shaw, A. L., Rothnagel, R., Chen, D., Ramig, R. F., Chiu, W., and Prasad, B. V. (1993). Three-dimensional visualization of the rotavirus hemagglutinin structure. *Cell* **74,** 693–701.

Sreerama, N., and Woody, R. W. (1994). Protein secondary structure from circular dichroism spectroscopy: Combining variable selection principle and cluster analysis with neural network, ridge regression, and self-consistent methods. *J. Mol. Biol.* **242,** 497–507, doi:10.1006/jmbi.1994.1597.

Stirzaker, S. C., Whitfield, P. L., Christie, D. L., Bellamy, A. R., and Both, G. W. (1987). Processing of rotavirus glycoprotein VP7: Implications for the retention of the protein in the endoplasmic reticulum. *J. Cell Biol.* **105,** 2897–2903.

Svensson, L., Dormitzer, P. R., von Bonsdorff, C. H., Maunula, L., and Greenberg, H. B. (1994). Intracellular manipulation of disulfide bond formation in rotavirus proteins during assembly. *J. Virol.* **68,** 5204–5215.

Takebe, M., Soe, G., Kohno, I., Sugo, T., and Matsuda, M. (1995). Calcium ion-dependent monoclonal antibody against human fibrinogen: Preparation, characterization, and application to fibrinogen purification. *Thromb. Haemostasis* **73,** 662–667.

Taniguchi, K., Hoshino, Y., Nishikawa, K., Green, K. Y., Maloy, W. L., Morita, Y., Urasawa, S., Kapikian, A. Z., Chanock, R. M., and Gorziglia, M. (1988). Cross-reactive and serotype-specific neutralization epitopes on VP7 of human rotavirus: Nucleotide sequence analysis of antigenic mutants selected with monoclonal antibodies. *J. Virol.* **62,** 1870–1874.

Tian, P., Estes, M. K., Hu, Y., Ball, J. M., Zeng, C. Q., and Schilling, W. P. (1995). The rotavirus nonstructural glycoprotein NSP4 mobilizes Ca^{2+} from the endoplasmic reticulum. *J. Virol.* **69,** 5763–5772.

Willis, S. H., Peng, C., Ponce de Leon, M., Nicola, A. V., Rux, A. H., Cohen, G. H., and Eisenberg, R. J. (1998). Expression and purification of secreted forms of HSV glycoproteins from baculovirus-infected insect cells. *In* "Methods in Molecular Medicine: Herpes Simplex Virus Protocols" (S. M. Brown and A. R. McLean, Eds.), Vol. 10. Humana Press, Totowa, NJ.

Yeager, M., Berriman, J. A., Baker, T. S., and Bellamy, A. R. (1994). Three-dimensional structure of the rotavirus haemagglutinin VP4 by cryo-electron microscopy and difference map analysis. *EMBO J.* **13,** 1011–1018.

Yeager, M., Dryden, K. A., Olson, N. H., Greenberg, H. B., and Baker, T. S. (1990). Three-dimensional structure of rhesus rotavirus by cryoelectron microscopy and image reconstruction. *J. Cell Biol.* **110,** 2133–2144.